ARTICLES
https://doi.org/10.1038/s41550-019-0756-5

nature astronomy

Corrected: Author Correction

A corridor of exposed ice-rich bedrock across Titan's tropical region

Caitlin A. Griffith[1*], Paulo F. Penteado[2,8], Jake D. Turner[3], Catherine D. Neish[4], Giuseppe Mitri[5], Nicholas J. Montiel[1], Ashley Schoenfeld[6] and Rosaly M. C. Lopes[7]

Global maps of Titan show great diversity in terrain types, but their associations with specific compositions on a large scale are obscured by Titan's thick atmosphere, which shrouds the weak spectral features. Here we develop a principal component analysis (PCA) that enables the identification of subtle spectral features. The PCA was applied to over 13,000 Cassini/VIMS spectra that cover half of Titan's globe, focused on tropical latitudes. Our analysis detected an ice-rich linear feature of bedrock, which extends a length equivalent to 40 per cent of Titan's circumference. This corridor is puzzling because it does not correlate with topography or measurements of the subsurface. Ice-rich terrains in other areas of Titan occur only in local regions excavated by craters or exposed by erosion, suggesting that cryovolcanism, if active, is currently not widespread. We also find evidence for a diversity of organic sediments, formed by the photolysis of Titan's past atmospheres, which remain to be investigated, perhaps using a similar approach.

Titan's density indicates an icy composition, like those of Saturn's other moons, which suggests that it has an icy surface too. However, Titan uniquely has an immense atmosphere composed mainly of N_2 and CH_4, which is photolysed in the upper atmosphere, thereby producing a plethora of organic molecules that end up as liquid and solid sediments on the surface[1]. Therefore, Titan's surface is expected to have two distinct components, an icy bedrock and the atmosphere-derived organic sediments[1].

Near-infrared investigations of Titan's surface

Titan's surface composition can be studied in the eight wavelength bands centred at 0.93 μm, 1.1 μm, 1.3 μm, 1.6 μm, 2.0 μm, 2.7 μm, 2.8 μm and 5.0 μm, between the optically thick CH_4 and CO bands in Titan's atmosphere (Fig. 1). Within these 'windows' candidate surface components exhibit characteristic absorption features; for example, NH_3 ice and C_2H_6 liquid absorb at 2.0 μm, while complex organic material may absorb at 0.93 μm and 1.08 μm (ref. [2]). However, water ice is the most straightforward constituent to identify, because three of its strong bands lie within the 1.6 μm, 2.0 μm and 2.8 μm windows[3].

Prior analyses of Titan's surface composition from spectral images of Cassini's Visual and Infrared Mapping Spectrometer (VIMS)[4] identified a broad range of terrain types. Examples include the spectrally distinct[5,6] dunes[7], craters marked with 1.6 μm and 2.0 μm absorptions characteristic of water ice[8], and a region surrounding Sotra Patera that morphologically resembles a cryovolcano[9]. These findings are achieved by analysing the reflectance, I/F, where I is the intensity of light at the top of Titan's atmosphere, and F is the incoming solar flux. The spectral nature of the surface is investigated either by mapping colour composites of several wavelengths[10], or of their fractions, sometimes including empirical corrections of the atmospheric scattering and surface photometry[11]. A principal component analysis (PCA) of the entire I/F spectrum has been conducted[12]. Additional studies targeted specific features[12] with radiative transfer (RT) models[12], which estimate the characteristics of haze and CH_4 opacity, and simulate the scattering and absorption of photons from the Sun as they pass through Titan's atmosphere, get reflected from Titan's surface, and emerge at the top of the atmosphere.

PCA investigation of Titan's surface

This project analyses the composition of the half of Titan's surface that is bounded by latitudes 30° S and 30°N (Supplementary Fig. 1) to study the surface spectral diversity and investigate the exposure of water-ice bedrock of Titan's tropical surface, despite the ongoing sedimentation of organic material from the atmosphere. Towards this goal, we developed a PCA analysis of the four wavelength bands (1.1 μm, 1.3 μm, 1.6 μm and 2.0 μm) that most clearly view Titan's surface from orbit.

In contrast to RT analyses, the PCA identifies and deconstructs the major spectral components based on the variance of the data. This approach, as discussed below, identifies the weak surface spectral features on a global scale without prior assumptions regarding the surface composition and atmospheric scattering and absorption, as assumed in RT analyses. A full RT analysis is significantly more time-consuming because the assumptions are evaluated at each spatial pixel. Rather than analysing each spectrum, one at a time, in detail, we study the correlations of the $M = 4{,}096$ spectra of a VIMS 'cube', each of which is recorded over 64×64 spatial pixels covering a contiguous region of Titan's surface. This analysis enables the identification of weak features by correlating the spectra. Of the $N = 4$ wavelength regions considered here, two (1.1 μm and 1.3 μm) reside outside H_2O absorptions and two (1.6 μm and 2.0 μm) are regions of H_2O absorption.

This work involves 37 VIMS cubes, which spatially overlap, each of which are analysed with the PCA independently (Supplementary

[1]Department of Planetary Sciences, LPL, University of Arizona, Tucson, AZ, USA. [2]Department of Physics and Astronomy, Northern Arizona University, Flagstaff, AZ, USA. [3]Department of Astronomy, University of Virginia, Charlottesville, VA, USA. [4]Department of Earth Sciences, University of Western Ontario, London, ON, Canada. [5]International Research School of Planetary Sciences, Università d'Annunzio, Pescara, Italy. [6]Department of Earth and Planetary Sciences, UCLA, Los Angeles, CA, USA. [7]Jet Propulsion Laboratory, California Institute of Technology, Pasadena, CA, USA. [8]Present address: Jet Propulsion Laboratory, California Institute of Technology, Pasadena, CA, USA. *e-mail: griffith@lpl.arizona.edu

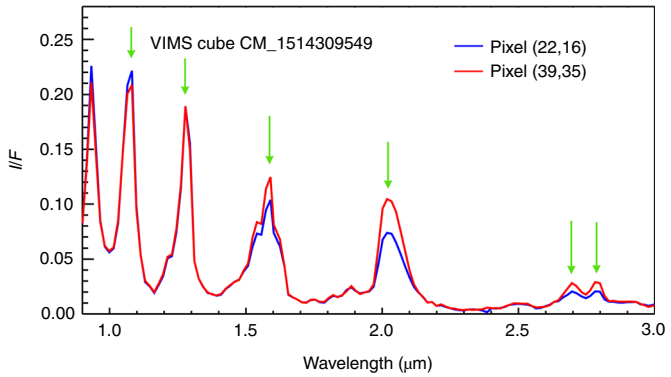

Fig. 1 | Two 0.9–3.0 μm VIMS spectra. Between Titan's strong atmospheric methane bands (the minimum points of the *I*/*F*) the atmosphere is transparent enough to probe Titan's surface. Six of these windows are used in this study (green arrows). We note that the blue spectrum (recorded at latitude 9.3° S, longitude 46.0° W) exhibits stronger absorptions at 1.6 μm and 2.0 μm than does the red pixel spectrum (5.5° S, 37.0° W). The PCA identifies the blue spectrum as having stronger ice absorptions than that of the red spectrum. The linewidth is wider than the s.d. error bars.

Table 1). We follow this protocol, because each VIMS cube samples different haze scattering, owing to the different lighting angles. The principal component axis defines the spectral trends that constitute the highest and therefore most obvious source of spectral variance, whereas successively lesser components indicate smaller sources of variance, and more subtle spectral trends of interest. The orthogonal spectral trends are derived by calculating the eigenvalues and eigenvectors of the $N \times N$ covariance matrix, $C_{i,j}$, defined by the I/F values (p_i) at the N window bands of each cube and their deviations from their mean values μ_i:

$$C_{i,j=}\frac{1}{M-1}\sum_M (p_i-\mu_i)(p_j-\mu_j) \quad (1)$$

The eigenvector associated with the highest eigenvalue defines the principal component, with successively smaller eigenvalues defining lesser sources of variance. Spectroscopically distinct terrains are identified by determining which spectra fit the principal component to within 1σ, and which of the remaining spectra require the second and third components to fit the data to within 1σ. Details of the methodology are given in the Methods.

The I/F distributions of the four wavelengths are not Gaussian, and introduce a slight displacement between the second eigenvector and the centre of the spread of the data points projected in this component. We therefore test our results against the RT analyses of local regions, and through the consistency of results in overlapping cubes. The third component is relevant in only one cube (1826075655), so the effects of the displacement are not compounded. Tests of our methodology and comparisons with other approaches are detailed in the Methods.

We target Titan's tropical surface, where the atmosphere is well characterized from in situ measurements by the Huygens probe at 10° S and 191° W (ref. [13]), thereby enabling comparisons of the PCA analysis with prior RT studies of several local regions.

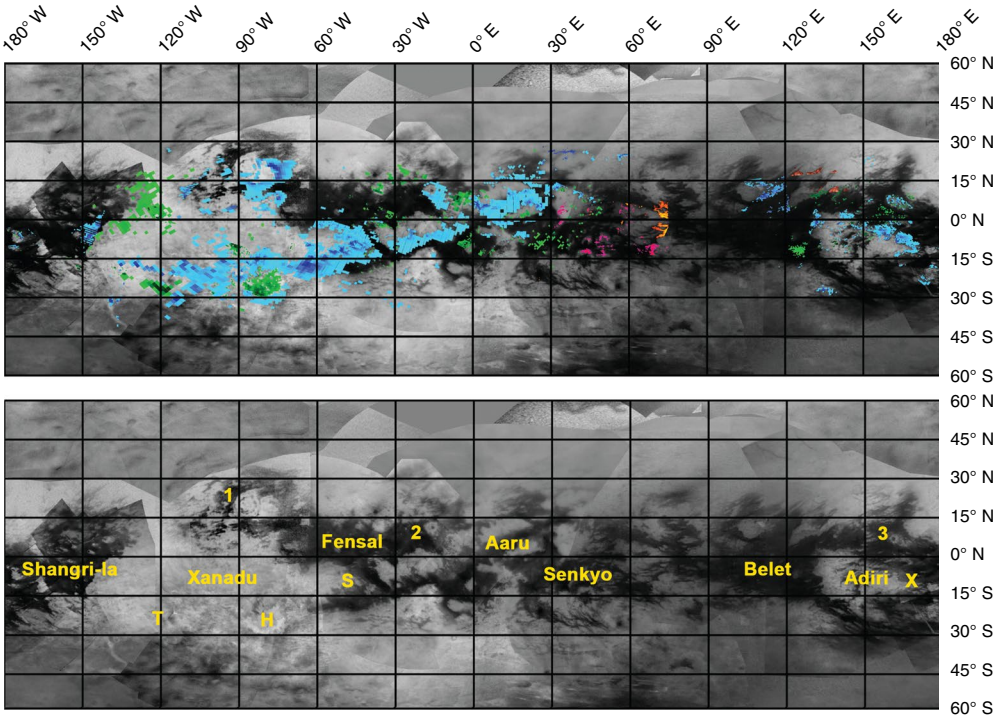

Fig. 2 | Composition map of Titan. The top panel shows the spectral trends derived from the PCA analysis of 37 VIMS cubes, at four window wavelengths. Blue pixels indicate ice-rich regions, that is, absorption at 1.6 μm and 2.0 μm, while green, red, orange and brown pixels indicate diverse ice-poor regions, with absorptions only at [1.1 μm and 1.3 μm], [1.1 μm], [2.0 μm], and [1.3 μm, 1.6 μm and 2.0 μm], respectively. These terrains overlay a Cassini/Imaging Science Subsystem (ISS) image at 0.93 μm wavelength. In the region covered by this PCA analysis (approximately 30° S to 30° N; Supplementary Fig. 1), the grey background indicates the average spectral trend, which matches the first component. The bottom panel shows the regions discussed in the text: the dark dune fields (for example, Fensal and Belet), the local regions of Sotra (S), Hotei Regio (H), Tui Regio (T), and the Huygens landing site (X), and three large craters: Menrva (1), Sinlap (2) and Selk (3). This map indicates that Titan's icy corridor and craters account for most of Titan's ice-rich surfaces. Credit: NASA/JPL-Caltech/Space Science Institute-PIA14908 (ISS image; https://go.nature.com/2G9CX0U).

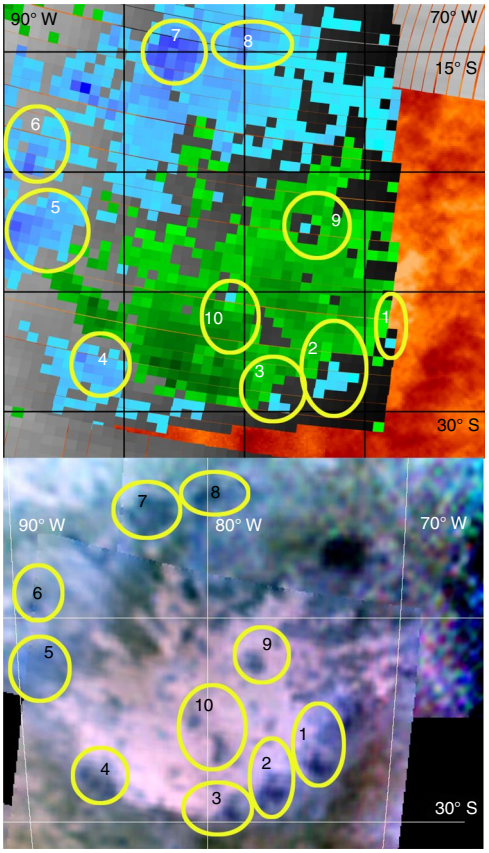

Fig. 3 | VIMS measurements of the second PCA component and an RT analysis of the Hotei Regio region. A comparison of the second PCA component (top) and the RT analysis[17] (bottom) shows that the ice-rich terrains (blue in both panels and numbered 1 to 10, and circled in yellow) match in detail, as do the ice-poor terrains (green in top panel and pink in bottom panel), indicating the consistency between the RT and PCA analyses. Reproduced from ref. [17], Elsevier (bottom).

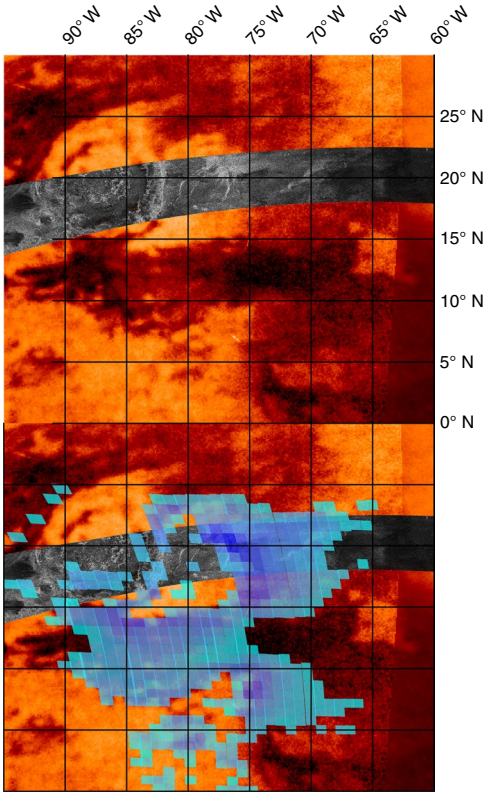

Fig. 4 | Titan's largest multi-ringed crater, Menrva, centred at 20° N latitude and 87° W longitude. The top panel shows a Cassini RADAR map (grey) from the T3 fly-by superimposed on a Cassini/ISS image at 0.93 μm wavelength. The bottom panel shows maps of the third PCA components. Blue regions indicate 1.6 μm and 2.0 μm absorptions.

The Cassini/VIMS cubes chosen for this analysis are detailed in the Supplementary Information. Each cube has an integration time greater than 60 s, which establishes the signal-to-noise ratio (S/N). The S/N values range from 25 to 50, for the bands used in the PCA analysis. We increase the S/N by averaging the I/F of two of the channels, channels 43 and 44 for the 1.6 μm band, and channels 70 and 71 for the 2.0 μm band. The 1.1 μm and 1.3 μm bands use the VIMS wavelength channels 13 and 25, respectively. To mitigate the effects of Titan's atmosphere, most cubes (30) have incident and scattering angles with cosine values above 0.40. However, to cover the regions of Hotei Regio and the terrain west of Menrva crater (Fig. 2), we include five cubes with incident and scattering angles having cosines ranging from 0.34 to 0.10, which yield consistent results with overlapping cubes at low scattering angles.

Spectral variance trends in tropical Titan

For all cubes, the principal component captures the main spectral trend of the surface, modulated by atmospheric scattering at different viewing angles and lighting conditions; that is, the major sources of variance in the datasets. The first component thereby finds the obvious surface spectral trends, and the effects of the atmosphere, precisely the information in which we are not interested. This component contains 87% to 99% of the variance, depending on the cube. The primary component carries the average surface spectrum, which, on the basis of Titan's 2.18 cm dielectric constant measured by Cassini/RADAR[14] and near-infrared studies (for example, refs. [15,16]) is dominated by organic sediments.

In contrast, the effects of Titan's atmosphere on the second component were found to be insignificant, as comparisons of overlapping cubes with different viewing angles and path lengths through Titan's atmosphere yield consistent results (Methods and Supplementary Fig. 2). Instead, the second component identifies weak spectral features of Titan's surface. We find that absorption features at 1.6 μm and 2.0 μm, characteristic of water ice, dominate the second component (Fig. 1). These signatures occur in 31 of the 37 cubes (Supplementary Table 1) and explain 0.4% to 13% of the spectral variance (Fig. 2, blue). The interpretation of water ice is further substantiated by studies of the cubes with the most direct viewing angles and lowest noise (Methods). These cubes reveal the subtle absorption feature at 2.8 μm, also characteristic of water ice (Supplementary Fig. 3). The features characteristic of water ice dominate the second component.

The second component also identifies spectral regions with the opposing trend to those with 1.6 μm and 2.0 μm absorptions; that is, spectra with absorptions at 1.1 μm and 1.3 μm. These short-wavelength absorptions, indicative of organic-rich, ice-poor terrains[8], appear in the Tui Regio[12] and Hotei Regio[17] regions (green areas in Figs. 2 and 3), areas of local, rather than global, depressions. Three additional spectral trends are found in the six variant cubes, which do not display ice features, and appear in ice-poor regions of Senkyo and Belet (yellow, magenta and purple areas in Fig. 2).

Distribution of water-rich and water-poor terrains

Our PCA study indicates that water ice is unevenly, but not randomly, exposed across Titan's tropical surface (Fig. 2). Most of the

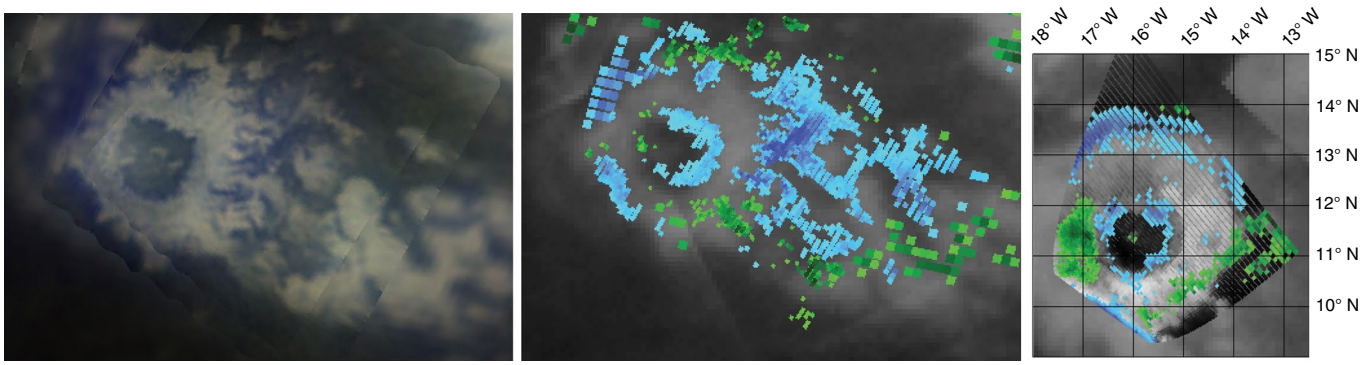

Fig. 5 | PCA analyses of the Selk and Sinlap craters. The left panel shows the surface albedos of Selk crater derived with a RT model[10]. The derived albedos at 2.0 μm, 1.6 μm and 1.3 μm are mapped in red, green and blue, respectively. The ice-rich regions are indicated in dark blue. Maps of the second PCA components of the Selk and Sinlap craters are shown in the middle and right panels, respectively. Blue regions indicate enhanced 1.6 μm and 2.0 μm surface absorption, while green regions indicate water-poor terrain. Reproduced from ref. [10], Elsevier (left).

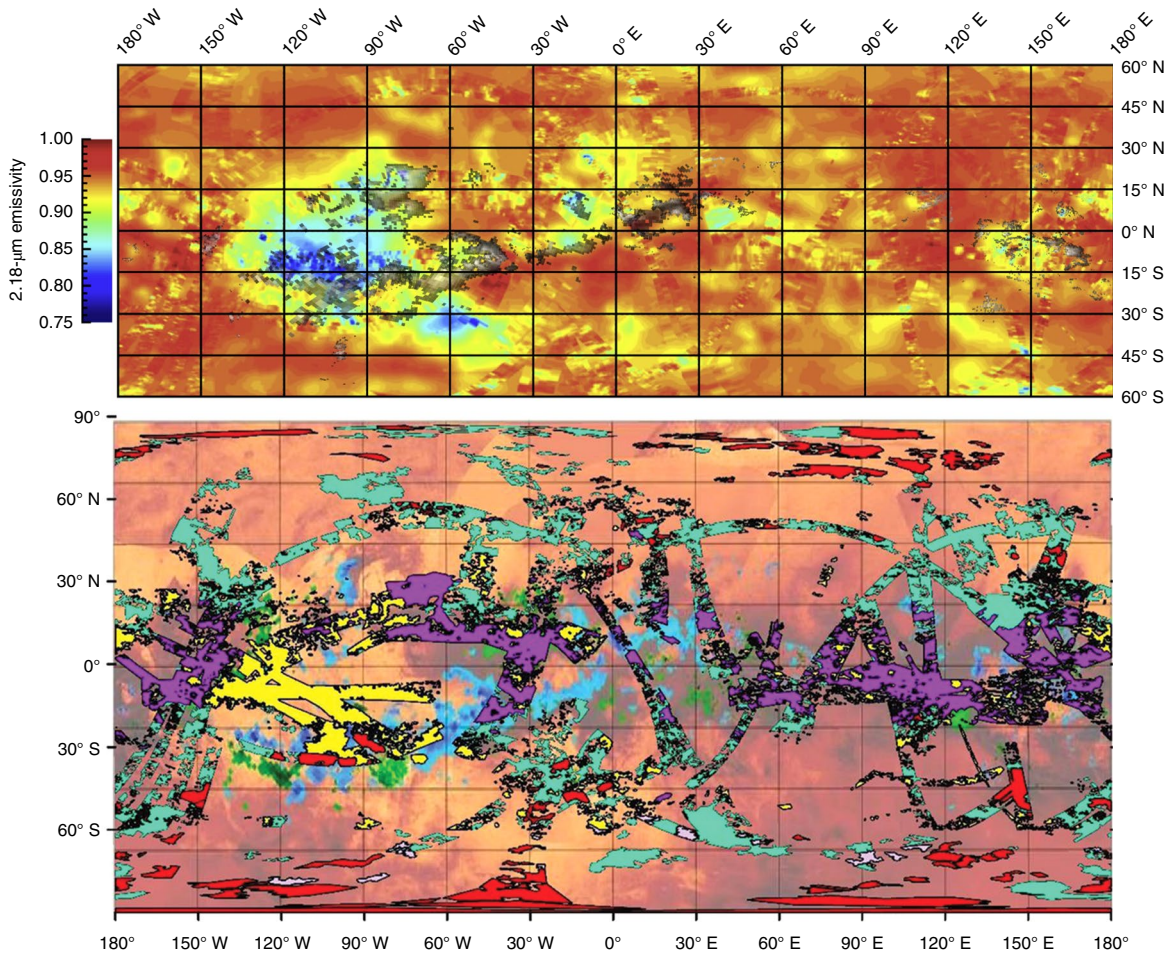

Fig. 6 | Radar maps compared to this study. The top panel shows the global emissivity map of Titan recorded by Cassini RADAR, indicating high to low emissivity with colours ranging from red to blue, respectively[20]. Superimposed upon this map are the water-ice-rich terrains indicated by the PCA analysis, here shown in black rather than blue for better visibility. The bottom panel shows the distribution of major geomorphologic units on Titan, including the undifferentiated plains (green), the dunes (purple), Labyrinth (red), and hummocky/mountainous terrains (yellow). The ISS global map is placed under the SAR swaths for context[36]. Superimposed on the RADAR map in blue are the ice-rich terrains identified by this PCA analysis of VIMS cubes. Adapted from ref. [14], Elsevier (top); and ref. [25], Elsevier (bottom).

exposed ice-rich material follows a long, nearly linear, corridor that stretches 6,300 km from roughly (30° E, 15° N) to (110° W, 15° S). Within this vast linear feature, we find the largest angular offsets between the second and first components, indicating the strongest water-ice features of Titan's tropical surface. The deepest ice absorptions occur in the Sotra complex (Fig. 2), a topographically unique

region, with a mountain 500 m high (Doom Mons) situated next to a pit 1,500 m deep, Sotra Patera, hypothesized to be of cryovolcanic origin[9]. The observations covering Sotra are at zenith viewing and have a high enough *S*/*N* to detect all three water-ice bands (1.6, 2.0 and 2.8 μm) in the low-lying dunes surrounding the Mohini Fluctus flow deposits (38.5° W, 11.8° S) that appear to emerge from Doom Mons (Supplementary Fig. 3). The surface distribution of organics-rich material indicates that aeolian and fluvial processes, which shape the dunes, work faster than the sedimentation of organic material, thereby potentially exposing ice-rich material[9,10]. However, it is unclear what connection, if any, exists between the 6,300-km-long linear feature and Sotra Patera, which is positioned roughly in the middle of the ice-rich corridor.

Titan's ice-rich corridor follows the margins of the dark dune fields and the bright terrain, extending from Sotra to Aaru (Fig. 2). Because Titan's dunes are truncated by locally steep elevations of the generally bright terrains[18,19], the bright-to-dark margins are likely to be escarpments, where high bright terrain looms over the dunes. Outside the Sotra-to-Aaru strip, the margins do not reveal ice, even when facing the same dune field as those that are icy. This omission indicates the presence of subsurface layers with variable compositions across Titan's tropical surface, where erosion into the dunes in some regions exposes otherwise buried water ice[8] (Supplementary Fig. 3). The correlation between ice-rich terrain and local topographical relief suggests erosional processes that expose and transport icy material to lowlands, where some of the icy terrain is currently found[8].

Outside this contiguous icy region, H_2O features make up a much smaller fraction of the total variance. The next-most-extensive region of enhanced water ice surrounds Titan's largest crater Menrva, with a diameter of 425 ± 25 km (ref. [20]). Exposed ice-rich material extends about 500 km to the east and southeast of the crater, a morphology that suggests an ejecta blanket, but one encroached on by dunes and highly eroded (Fig. 4). Yet here the 1.6 μm and 2.0 μm spectral features appear in the third component, and carry only 0.75% of the variance. The detection of these features is enabled by the PCA analysis, which samples the correlations of thousands of spectra in the cube. The weak nature of the ice features suggests a mixture of icy and non-icy components, perhaps caused by erosion, consistent with the aeolian and fluvial processes indicated by Cassini RADAR images[21,22]. Scattered regions of weak ice enhancement also surround smaller craters (Fig. 5) and the Adiri terrain, again principally along the margins of the dark and bright terrains. This region encompasses the Huygens probe landing site (Fig. 2) where we detect faint ice features, consistent with in situ measurements by the Huygens probe[13] and VIMS measurements[23].

A comparison of our results with Cassini RADAR measurements of Titan's emissivity at 2.18 cm (refs. [14,24]) indicates similarities in the exposure of water ice, with inconsistencies probably caused by the low resolution of some of the RADAR data and the different levels probed by the different wavelengths. Titan's ice-rich corridor, according to synthetic aperture radar (SAR) studies of the surface morphology[25], correlates with some of the oldest terrains on Titan's surface (Fig. 6). These terrains appear ice-rich in composition, with active mass wasting and weathering effectively clearing the surface of more recent organic deposits[26].

Implications

Titan's global ice feature presents a puzzle. It does not correlate in any obvious way with the Bouguer gravity anomaly, a measure of the gravitation field and therefore of the material below the subsurface[27], nor does it correlate with topography, as measured from Cassini RADAR measurements[19]. However, gravity measurements have been conducted only at low spatial resolution, and topography measurements are sparse. The linearity of the icy corridor over a global scale presents the question of whether tectonic processes shaped this feature, thereby manifesting the processes that mould Titan's surface and subsurface on a global scale. However, we find no evidence that Titan is geologically active, consistent with Titan's long-wave topography and gravity field, which indicate a thick ice shell that is conductive rather than convective[27,28].

The ice-poor terrains detected in the second PCA component (Fig. 2) indicate compositionally diverse organic sediments. These surface deposits are of interest because laboratory simulations of Titan's atmosphere produce amino acids[29] that potentially reside on Titan's surface. Further analyses of all window wavelengths can explore the possibility that this heterogeneity arises from chemical or physical evolution of the sediments[3].

The history of Titan's interior and atmosphere bear on the distribution and abundances of organic sediments. Measurements of the $^{13}C/^{12}C$ ratio in Titan's atmosphere[30] indicate that methane was injected into the atmosphere not more than 0.5–1 billion years ago. This age is consistent with the volume of dunes that would have accumulated since then, and suggest, consistent with evolution models of Titan's interior[31], that a major cryovolcanic event occurred several million years ago[32]. Potentially the topography that established the steep slopes of the icy corridor is a remnant of the time when Titan was geologically active. One example is the Sotra region, which displays cryovolcanic features, the steep terrain of which exhibits the strongest water-ice features.

The communication between the surface and the interior probably plays a major part in Titan's current surface and atmosphere. This is indicated by the paucity of liquid methane on Titan's surface (less than that in the atmosphere) which through evaporation supplies atmospheric CH_4. Without an additional, source Titan's CH_4 will be exhausted in just 20 million years. Yet a longstanding lake in Titan's tropical desert[33] indicates that subsurface reservoirs also supply methane to Titan's atmosphere, thereby prolonging the methane atmosphere and accumulation of sediments.

Additional studies of Titan's surface, concerning outgassing[34], the terrain ages, detailed topography and gravity maps and surface composition, are needed to address the larger question of whether prolonged production of complex organics, sourced by subterranean reservoirs, are common in cool CH_4-rich exoplanetary atmospheres.

Methods

Details of the methodology. Our analysis most resembles the three-dimensional rotation of 4,096 *I*/*F* values of three window wavelengths (1.3 μm, 1.6 μm and 2.0 μm) of the CM1514302573 cube, by Soderblom et al. [8]. Their rotation of the *I*/*F* values was conducted by hand to study the variance of the data. The PCA, in contrast, systematically calculates the eigenvalues and eigenvectors of the covariance matrix. It enables studies of weaker features, larger datasets, and the correlations of spectra involving more than three wavelengths, thereby complementing the detailed but lengthy RT analysis.

The PCA identifies the orthonormal eigenvectors according to the variance of the data. The angular offset of the second component onto the principal component, for each pixel, indicates the spectral contributions of the second component spectrum compared to that of the principal component. The *I*/*F* angular offsets of the second component from the principal component have two senses, when projected onto the first component (Supplementary Fig. 4). We find that for most cubes the second component indicates spectra that have 1.6 μm and 2.0 μm absorptions and 1.6 μm and 2.0 μm peaks. Only rarely do we find other spectral trends, such as a 1.6 μm peak and 2.0 μm absorption.

For a given spatial pixel, if the first component does not fit the data to within 1σ, we then add the second component and determine whether the combined first and second components fit the data to within 1σ. If these two components explain the data within the errors, then we discern how the second component modifies the first component spectral trend. If the second component, when added to the first component, indicates absorption at 1.6 μm and 2.0 μm, then the pixel is blue, indicative of water-rich terrain. The tint of the blue colour reflects the degree of the *I*/*F* angular offsets of the second component. If, instead, the angle between the first and second components indicates less 1.6 μm and 2.0 μm absorption, the pixel is designated green, indicative of a relatively water-poor surface. Only in the Menrva cube (1826075655) do ice absorptions occur in the third component. The angular offsets that are above the noise for the approximately 130,000 spatial pixels are given in Supplementary Fig. 4. Supplementary Table 1 provides details of each cube and its analysis.

Validation of our technique. The VIMS cubes were chosen such that the footprint of each cube overlies the neighbouring cubes. This redundancy enables us to assess whether the PCA extracts the effects of Titan's overlying atmosphere. We compare the PCA results of the overlying sections that sample the same terrain, but have different viewing angles. We find that results in the overlapping segments are fully consistent, as shown for the six cubes near (60° W,0° S) (Supplementary Fig. 2).

To test the results of our methodology, we compare the results of the PCA analysis to those of a full discrete ordinates RT analysis[35], which include studies of the errors. Two studies enable a detailed comparison to our work, because they map the derived surface albedo to each VIMS pixel, and include a study of the uncertainties of the atmospheric effects. These cubes cover Hotei Regio[17], a 500-km-across, semi-circular basin[36] located at (25° S, 80° W), and the 80-km-across Selk crater, situated at (26° N, 200° W).

The PCA and RT analyses of Hotei Regio yield consistent results, with detailed agreement of the location of the water-rich and water-poor terrains (Fig. 3). Both studies find that the basin has a water-poor surface. In contrast, water-rich regions occur at the base of drainage systems in small local depressions southeast of Hotei Regio, and in a larger region north of Hotei Regio[17]. The ice-rich material has been interpreted to be fluvial deposits, eroded and transported by liquid methane[17], and therefore a local effect.

Likewise, both PCA and RT studies of Selk crater consistently indicate that water-rich ice encircles the crater's outer rim, and extends eastward of the crater in a sinuous pattern[37] (Fig. 5). These features suggest erosion in the west flank of the rim, and a highly eroded ejecta blanket, potentially sculpted by methane rain. While the Selk crater appears therefore to be a somewhat eroded crater[37], the strong ice enrichment that defines the crater rim indicates a less gardened crater than Menrva, suggesting that Selk was formed from a more recent impact[38]. These studies and RT analyses that analyse specific spectra[12] agree fully with the PCA analysis.

Evidence of water ice. Water ice has strong absorption features at 1.6 μm, 2.0 μm and 2.8 μm. However, owing to the weakness of the latter feature and the accompanying noise, it is difficult to identify its signature. At 2.8 μm, Titan has a low surface albedo, which coupled with the high absorptivity of Titan's atmosphere at these wavelengths, leads to *I*/*F* values are 4–9 times lower than those at wavelengths 1.1 μm, 1.3 μm, 1.6 μm and 2.0 μm (Fig. 1). The variance of the *I*/*F* values at 2.7 μm and 2.8 μm are therefore comparatively small and noisy and thus inappropriate for this PCA analysis.

To test the assumption that the 1.6 μm and 2.0 μm absorptions are indeed due to water ice, we examine whether the terrains that exhibit the 1.6 μm and 2.0 μm absorptions, based on the PCA analysis, also exhibit the 2.8 μm absorption. Instead of using a PCA, we divide the 2.8 μm *I*/*F* values by those at 2.7 μm, where water absorption is weaker[3]. To increase the *S*/*N*, we average the *I*/*F* of channels 110 and 111 for the 2.7 μm band, and channels 116 and 117 for the 2.8 μm band. Ice-rich regions are indicated where the 2.8 μm to 2.7 μm *I*/*F* ratio is low, owing to 2.8 μm absorption.

However, unlike past work that failed to detect the strong 2.8 μm feature[3], we consider only the cubes (Adiri 1567240658, Sinlap 1790056808 and Sotra 1514309549) that have a nearly zenith viewing of the surface, and a high *S*/*N*, that is, a low incidence of the scattering angles ≤20° and exposure times ≥160 s. The low viewing angles are critical, because Titan's atmospheric CH_4 absorbs more strongly at 2.7 μm than at 2.8 μm. At high path lengths, therefore, Titan's atmosphere more strongly depresses the 2.7 μm *I*/*F*, which can lead to misleading results such as the impression that the surface albedo is lower at 2.7 μm than at 2.8 μm (ref. [39]).

This study reveals that for each of the three zenith-viewing cubes, the presence of a strong 2.8 μm absorption feature correlates with the presence of the 1.6 μm and 2.0 μm water-ice signatures, as shown for the Sotra cube in (Supplementary Fig. 3). The drop in the 2.8 μm absorption from that at 2.7 μm was found to be at most 10%. The *I*/*F* standard deviation at 2.7–2.8 μm is 0.001 and the maximum *I*/*F* value is 0.011. The detection of 2.8 μm absorption at each pixel is at the 1σ level. At *I*/*F* values below 0.0048, characteristic of the dark dunes, the 2.8 μm absorption feature is below the 1σ level. Therefore the 2.8 μm absorption cannot be measured well in the dunes with this technique, and discrepancies arise between the PCA analysis and the simple 2.7 μm to 2.8 μm *I*/*F* ratio (Supplementary Fig. 3). For the other cubes examined here the 2.8 μm absorption lies below the 1σ level, because of the higher noise level and muted nature of the surface spectra as viewed through higher atmospheric paths.

We note that the interpretation that the 1.6 μm and 2.0 μm absorptions are due to water ice is supported by the detection of these features in the ejecta blankets of craters (for example, Menrva, Sinlap and Selk). These impacts excavated material tens of kilometres deep, that is, well below the organic sediment layer and into Titan's icy bedrock[40,41].

Comparison with prior studies. The Sinlap crater, which has a 82 ± 2 km diameter and is 640 ± 160 m deep[40], has been analysed extensively, using different methods. It thereby provides opportunities to compare different techniques. Prior studies detect 1.6 μm and 2.0 μm absorptions, as well as a high dielectric constant[14] indicative of an extended region of exposed water ice[8] southwest of the crater (Figs. 2 and 5). This region is interpreted as the crater's ejecta blanket, formed by the impact of an object about 7 km across, which caused ballistic ejecta and a vapour plume from which small particles condensed and drifted downwind[40].

The composition of Sinlap, studied from RT analyses[12], match our PCA results, while colour composite analyses[10] agree with most but not all features, as indicated by a close-up VIMS measurement (Fig. 5). For example, the PCA does not find enhanced ice on the crater floor, as indicated by the colour composites[41]. Yet studies of the composites of the fractions of several wavelengths[40] that include empirical corrections of the atmospheric scattering are consistent with our work on Sinlap. Recent maps of Titan's globe, similarly constructed, indicate (in dark blue) the features that we detect as water ice, with the exception of the region around 15° E longitude and 8° N latitude. PCA and RADAR and colour composite analyses[40] also indicate erosion and a slumping of part of the northern rim. We find that the strongest water features follow most of the inner rim of the crater, while the floor and the ejecta blanket are relatively ice-poor (Fig. 5), consistent with the accumulation of organic material on the crater floor. The ejecta blanket may represent an intimate mixture of organic material and water ice, formed during the high-energy impact event[40] with subsequent mass wasting revealing ice-rich surfaces on the steep crater rim wall. The edge of the icy ejecta blanket lies to the northwest[40]. Sinlap's highly intact ejecta blanket footprint and strong ice features suggest a younger crater than both Menrva and Selk[41].

These studies indicate that the PCA matches prior RT analyses in detail. The empirical method that corrects for scattering and surface photometry[40] agrees with our PCA well, while maps of colour composites mostly yield similar results. The disparities are largest over Titan's dark terrains and highly scattering viewing angles, effects that are extracted by the PCA's principal component.

Data availability

The Cassini data analyszed in this work are available through the Planetary Data System (https://pds.nasa.gov). The data that support the plots within this paper and other findings of this study are available from the corresponding author upon reasonable request.

Received: 23 August 2017; Accepted: 13 March 2019;
Published online: 29 April 2019

References

1. Yung, Y. L., Allen, M. & Pinto, J. P. Photochemistry of the atmosphere of Titancomparison between model and observations. *Astrophys. J. Suppl. Ser.* **55**, 465–506 (1984).
2. Cruikshank, D. P. et al. Solid C triple bond N-bearing material on outer Solar System bodies. *Icarus* **94**, 345–353 (1991).
3. Clark, R. N. et al. Detection and mapping of hydrocarbon deposits on Titan. *J. Geophys. Res. Planets* **115**, 10005 (2010).
4. Brown, R. H. et al. The Cassini Visual and Infrared Mapping Spectrometer (VIMS) investigation. *Space Sci. Rev.* **115**, 111–168 (2004).
5. Barnes, J. W. et al. Spectroscopy, morphology and photoclinometry of Titan's dune fields from Cassini/VIMS. *Icarus* **57**, 400–414 (2008).
6. Le Gall, A. et al. Cassini SAR, radiometry, scatterometry and altimetry observations of Titan's dune fields. *Icarus* **213**, 608–624 (2011).
7. Lorenz, R. D. et al. The sand seas of Titan: Cassini RADAR observations of longitudinal dunes. *Science* **312**, 724–727 (2006).
8. Soderblom, L. A. et al. Correlations between Cassini VIMS spectra and RADAR SAR images: implications for Titan's surface composition and the character of the Huygens probe landing site. *Planet. Space Sci.* **55**, 2025–2036 (2007).
9. Lopes, R. M. C. et al. Cryovolcanism on Titan: new results from Cassini RADAR and VIMS. *J. Geophys. Res. Planets* **118**, 416–435 (2013).
10. Barnes, J. W. et al. Global-scale surface spectral variations on Titan seen from Cassini/VIMS. *Icarus* **186**, 242–258 (2007).
11. Le Mouélic, S. et al. The Cassini VIMS archive of Titan: from browse products to global infrared color maps. *Icarus* **319**, 121–132 (2019).
12. Solomonidou, A. et al. Surface albedo spectral properties of geologically interesting areas on Titan. *J. Geophys. Res. Planets* **119**, 1729–1747 (2014).
13. Tomasko, M. G. et al. Rain, winds and haze during the Huygens probe's descent to Titan's surface. *Nature* **438**, 765–778 (2005).
14. Janssen, M. A. et al. Titan's surface at 2.18-cm wavelength imaged by the Cassini RADAR radiometer: results and interpretations through the first ten years of observation. *Icarus* **270**, 443–459 (2016).
15. Radebaugh, J. et al. Dunes on Titan observed by Cassini RADAR. *Icarus* **194**, 690–703 (2008).
16. Bonnefoy, L. et al. Compositional and spatial variations in Titan dune and interdune regions from Cassini VIMS and RADAR. *Icarus* **207**, 222–237 (2016).
17. Soderblom, L. A. et al. The geology of Hotei Regio, Titan: correlation of Cassini VIMS and RADAR. *Icarus* **204**, 610–618 (2009).
18. Lorenz, R. D. & Radebaugh, J. Global pattern of Titan's dunes: radar survey from the Cassini PRIME mission. *Geophys. Res. Lett.* **36**, L03202 (2009).

19. Lorenz, R. D. et al. A global topographic map of Titan. *Icarus* **225**, 367–377 (2013).
20. Neish, C. D. et al. Crater topography on Titan: implications for landscape evolution. *Icarus* **223**, 82–90 (2013).
21. Lopes, R. M. C. et al. Distribution and interplay of geologic processes on Titan from Cassini RADAR data. *Icarus* **205**, 540–558 (2010).
22. Williams, D. A., Radebaugh, J., Lopes, R. M. C. & Stofan, E. Geomorphologic mapping of the Menrva region of Titan using Cassini RADAR data. *Icarus* **212**, 744–750 (2011).
23. Rodriguez, S. et al. Cassini/VIMS hyperspectral observations of the HUYGENS landing site on Titan. *Planet. Space Sci.* **54**, 1510–1523 (2006).
24. Ostro, S. J. et al. Cassini RADAR observations of Enceladus, Tethys, Dione, Rhea, Iapetus, Hyperion, and Phoebe. *Icarus* **183**, 479–490 (2006).
25. Lopes, R. M. C. et al. Nature, distribution, and origin of Titan's undifferentiated plains. *Icarus* **270**, 162–182 (2016).
26. Werynski, A., Neish, C. D., Gall, A. L., Janssen, M. A. & the Cassini Radar Team. Compositional variations of Titan's impact craters indicate active surface erosion. *Icarus* **321**, 508−521 (2019).
27. Mitri, G. et al. Shape, topography, gravity anomalies and tidal deformation of Titan. *Icarus* **236**, 169–177 (2014).
28. Nimmo, F. & Bills, B. G. Shell thickness variations and the long-wavelength topography of Titan. *Icarus* **208**, 896–904 (2010).
29. Hörst, S. M. et al. Formation of amino acids and nucleotide bases in a titan atmosphere simulation experiment. *Astrobiology* **12**, 809–817 (2012).
30. Mandt, K. E. et al. The $^{12}C/^{13}C$ Ratio on Titan from Cassini INMS measurements and implications for the evolution of methane. *Astrophys. J.* **749**, 160 (2012).
31. Tobie, G., Lunine, J. I. & Sotin, C. Episodic outgassing as the origin of atmospheric methane on Titan. *Nature* **440**, 61–64 (2006).
32. Sotin, C. et al. Observations of Titan's northern lakes at 5 μm: implications for the organic cycle and geology. *Icarus* **221**, 768–786 (2012).
33. Griffith, C. A. et al. Possible tropical lakes on Titan from observations of dark terrain. *Nature* **486**, 237–239 (2012).
34. Solomonidou, A. et al. Temporal variations of Titan's surface with Cassini/VIMS. *Icarus* **270**, 85–99 (2016).
35. Griffith, C. A. et al. Radiative transfer analyses of Titan's tropical atmosphere. *Icarus* **218**, 975–988 (2012).
36. Stiles, B. W. et al. Determining Titan surface topography from Cassini SAR data. *Icarus* **202**, 584–598 (2009).
37. Soderblom, J. M. et al. Geology of the Selk crater region on Titan from Cassini VIMS observations. *Icarus* **208**, 905–912 (2010).
38. Neish, C. D. et al. Strategies for detecting the products of aqueous chemistry on Titan. In *Lunar Planet. Sci. Conf.* **48**, 1457 (2017).
39. Hayne, P. O., McCord, T. B. & Sotin, C. Titan's surface composition and atmospheric transmission with solar occultation measurements by Cassini VIMS. *Icarus* **243**, 158–172 (2014).
40. Le Mouélic, S. et al. Mapping and interpretation of Sinlap crater on Titan using Cassini VIMS and RADAR data. *J. Geophys. Res. Planets* **113**, 4003 (2008).
41. Neish, C. D. et al. Spectral properties of Titan's impact craters imply chemical weathering of its surface. *J. Geophys. Res. Planets* **42**, 3746–3754 (2015).

Acknowledgements

C.A.G.'s research is partially funded by NASA's Cassini Program. J.T. and N.J.M.'s work were funded by NASA space grants. P. Penteado was supported by the Northern Arizona University Office of the Vice President for Research. We thank L. Soderblom for discussions on Titan's geology, and L. Palafox for his discussions on the blind source separation.

Author contributions

C.A.G. developed, tested and interpreted the PCA analysis and led all aspects of the project. P.F.P. accessed and reduced all the Cassini data. J.T. and N.M. combed the Cassini data bank for viable and scientifically interesting cubes. G.M. contributed to the discussion of the ice-rich feature. C.D.N. contributed to the discussion of craters and other aspects of Titan's geology. A.S. and R.M.C.L. put together the map of the distribution of major geomorphologic units on Titan (Fig. 6, bottom panel).

Competing interests

The authors declare no competing interests.

Additional information

Supplementary information is available for this paper at https://doi.org/10.1038/s41550-019-0756-5.

Reprints and permissions information is available at www.nature.com/reprints.

Correspondence and requests for materials should be addressed to C.A.G.

Journal peer review information: *Nature Astronomy* thanks Sylvain Douté and the other anonymous reviewer(s) for their contribution to the peer review of this work.

Publisher's note: Springer Nature remains neutral with regard to jurisdictional claims in published maps and institutional affiliations.